CHINESE OPTICS LETTERS

Vol. 21, No. 10 | October 2023

Photothermal nonlinear scattering of shell-isolated gold nanoparticles and applications in super-resolution imaging

Tianyue Zhang (张天悦)[1,2*], Zhiyuan Wang (王知远)[1], Xiangchao Zhong (钟祥超)[1], Ying Che (车 颖)[1], and Xiangping Li (李向平)[1**]

[1] Guangdong Provincial Key Laboratory of Optical Fiber Sensing and Communications, Institute of Photonics Technology, Jinan University, Guangzhou 510632, China

[2] School of Integrated Circuits, Beijing University of Posts and Telecommunications, Beijing 100876, China

*Corresponding author: tyzhang@jnu.edu.cn

**Corresponding author: xiangpingli@jnu.edu.cn

Received February 7, 2023 | Accepted May 5, 2023 | Posted Online August 30, 2023

In this Letter, we report on the investigations of nonlinear scattering of plasmonic nanoparticles by manipulating ambient environments. We create different local thermal hosts for gold nanospheres that are immersed in oil, encapsulated in silica glass and also coated with silica shells. In terms of regulable effective thermal conductivity, silica coatings are found to contribute significantly to scattering saturation. Benefitting from the enhanced thermal stability and the reduced plasmonic coupling provided by the shell-isolated nanoparticles, we achieve super-resolution imaging with a feature size of 52 nm ($\lambda/10$), and we can readily resolve pairs of nanoparticles with a gap-to-gap distance of 5 nm.

Keywords: noble metal nanoparticles; plasmonic scattering; effective thermal conductivity; super-resolution.
DOI: 10.3788/COL202321.103601

1. Introduction

Plasmonic nanoparticles with localized surface plasmon resonance (LSPR) are famously known as excellent scatterers and absorbers of light[1], mediating various applications in chemical and biomolecular sensing, energy harvesting, data storage, and optical imaging[2]. In particular, plasmonic nanoparticles have recently been explored as image contrast agents for optical super-resolution imaging[3,4], offering benefits such as size- and shape-tunable optical responses, high photostability, bright signals, and lack of blinking. Moreover, novel super-resolution imaging techniques relying on these plasmonic absorption and scattering properties provide non-fluorescent schemes for breaking the diffraction limit in far-field nanoimaging.

Plasmonic scattering of metallic nanoparticles has been reported to show nonlinear power dependences of scattering on excitation laser intensities[5]. Theoretical and experimental studies have demonstrated that the nonlinear behavior originates from the plasmon-enhanced light absorption and the subsequent thermal effects[6–8]. The large photothermal nonlinearity of plasmonic scattering allows for the implementation of super-resolving strategies. For instance, saturated scattering has been used to achieve the super-resolution of gold nanoparticles by extracting the nonlinear components in the scattering signal via temporal modulation and demodulation[5,9]. Photoswitching of plasmonic nonlinear scattering has been observed and employed to resolve single nanoparticles within a diffraction-limited spot by using a donut beam to photothermally suppress the scattering signal in the periphery of the focus[10,11].

The nonlinearity of plasmonic scattering has been widely observed in various structures, such as nanospheres[5,10–13], nanorods[14], nanoshells[9], and nanostars[15], as well as different materials like gold and silver. Since the scattering nonlinearity of the nanoparticles is attributed to the photothermally induced changes in the optical properties, the thermal conductivity of the local surrounding medium associated with the heat dissipation is crucial. However, previous studies about nonlinear plasmonic scattering have seldom reported on the effects of the immediate surroundings (via the thermal conductivity), and the experimental demonstration of engineering the local thermal environment is still very lacking.

In this Letter, we compared the saturated scattering of gold nanospheres immersed in oil, embedded in silica glass, and coated with silica shells to create different thermal hosts, and we achieved the super-resolution imaging of core-shell nanoparticles using suppression of scattering imaging (SUSI) microscopy. Silica coatings with different shell thicknesses were observed to contribute significantly to local thermal conductivity of the gold core and also to the particle thermal stability. Compared with the bare gold nanospheres, the shell-isolated gold nanoparticles are not only photothermally more stable

but also can effectively prevent plasmon coupling due to particle aggregations. This enables us to access the super resolving of two individual shell-isolated nanoparticles with the gap-to-gap distance of 5 nm. The full-width at half-maximum (FWHM) of the measured image spot from the single core-shell nanoparticle (70 nm gold core with 40 nm silica shell) can be squeezed to 52 nm ($\sim\lambda/10$). Our results provide insights for the crucial role that local heat dissipation plays on nonlinear plasmonic scattering and can potentially benefit super-resolution optical imaging in biology systems using plasmonic core-shell nanoparticles as scattering nanoprobes.

2. Sample Preparation and Optical Measurements

In our study, we concentrated on gold nanospheres (AuNSs) and prepared several samples containing AuNSs within different surroundings for nonlinear scattering measurements [Fig. 1(a)]. Gold nanospheres of 70 nm in diameter were wet-chemically synthesized using the citrate-reduced method in an aqueous solution. Core-shell nanoparticles (denoted as Au@SiO_2) with 70 nm gold core and silica shell thickness of 10 nm, 23 nm, and 40 nm were purchased from NanoLab (Xiamen Luman Technology Co., Ltd.). The nanoparticles (bare AuNSs and Au@SiO_2) were first deposited onto the glass coverslip, then immersed in the index-matching oil, and then finally sealed by a cover glass. In addition, the as-deposited AuNSs were also sealed with a commercial spin-on glass (SOG) material (IC1-200, Futurrex) to create the infinite silica encapsulating[16]. To this extent, the AuNSs in all cases are in the same optical environment due to the homogenous medium dielectric constant, but they experience different local thermal environments caused by varied immediate surroundings during optical heating.

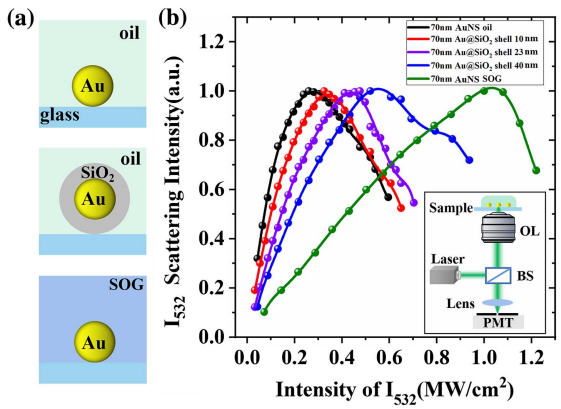

Fig. 1. (a) Schematic illustration of the different local thermal environments created for 70-nm-diameter gold nanospheres. (b) Experimental measurements of nonlinear plasmonic scattering of the five prepared samples, showing the nonlinear dependency of scattering on irradiance intensities for continuous-wave excitations at the wavelength of 532 nm. The optical setup of the reflected laser scanning confocal microscope is shown in the inset. BS, beam splitter; OL, objective lens; PMT, photomultiplier tube.

The experimental setup was based on the Abberior 775 STED confocal microscope (Abberior Instruments GmbH, Göttingen)[11]. We coupled a continuous-wave laser line (532 nm) into the system in order to resonantly excite the nanoparticles for nonlinear scattering measurements [see the inset in Fig. 1(b)]. For super-resolution imaging experiments, a vortex phase plate was inserted in the light path to convert the 532-nm-laser beam into a donut shape. The 561-nm Gaussian excitation beam and the donut beam were coaligned and focused onto the nanoparticles through the objective lens (Olympus, UPlanSApo 100 × /NA = 1.4, oil immersion), and sub-diffraction-limited images were acquired by beam scanning with a pixel size of 6 nm and 10 μs dwell time using the software Imspector (Abberior Instruments).

3. Results and Discussion

Figure 1(b) shows the remarkable differences in nonlinear scattering behaviors for the prepared five samples. The experimental results illustrate that bare AuNSs in oil reach saturation first, followed by the core-shell nanoparticles with shells of 10 nm, 23 nm, and 40 nm, while the AuNSs in the SOG material arrive at scattering saturation at the highest laser intensity. The incident light power required for the scattering saturation of 70 nm AuNSs in the above five local microenvironments was 0.25 MW/cm^2, 0.3 MW/cm^2, 0.4 MW/cm^2, 0.55 MW/cm^2, and 1.0 MW/cm^2, respectively. The AuNSs in all the samples have the same surrounding refractive index, meaning that the nanoparticles in all the cases have the same LSPR peak. Moreover, we have also proved through calculations that there is almost no difference in the absorption cross sections of all these nanoparticles. Hence, the variations in the nonlinear temperature rise and scattering responses are attributed to the thermal effects related to the heat conduction associated with the effective thermal conductivity (κ_{eff}) that takes both the substrate and the environment into account[8,17,18].

As artistically illustrated in Fig. 2(a), under resonant laser irradiation, the plasmon-enhanced absorption induces optical heating of the nanoparticles, and the final temperature increase depends strongly on the local surrounding media via the effective thermal conductivity, which governs the heat dissipation. Considering that the sufficient temperature rising affects the metal permittivity and permittivity change in turn causes absorption and scattering efficiency variation, the heating process becomes nonlinear and needs to be solved iteratively. Therefore, we perform the theoretical calculations of nonlinear scattering of the gold nanoparticles by harnessing the temperature-dependent permittivity model[19], as well as taking local thermal environments into account by evaluating different κ_{eff}. In the case of the AuNSs on the glass substrate and sealed within the immersion oil, κ_{eff} was taken to be 0.3 W/mK. For the AuNSs on the glass substrate and encapsulated in the SOG materials, κ_{eff} was taken to be 1 W/mK. For the AuNSs coated with different thicknesses of silica shell, κ_{eff} was estimated to be intermediate values.

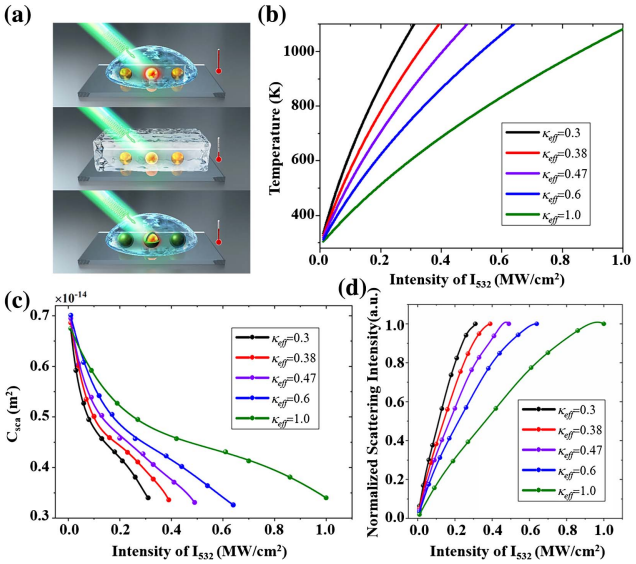

Fig. 2. (a) Illustration of optical heating of the gold nanospheres that converts light into temperature rises. Due to the difference in the local thermal media, the gold nanospheres (top, in immersion oil; middle, in SOG materials; and bottom, with silica coatings) undergo various temperature rising. (b) Theoretical calculations of the temperature evolution of a single 70-nm-diameter gold nanosphere surrounded by different thermal host media characterized by κ_{eff} and subject to CW laser illumination with increasing laser intensity I_{532}. (c) The evolution of the scattering cross sections of the gold nanospheres with excitation intensities. (d) The calculated plasmonic scattering intensities of the gold nanospheres as a function of 532 nm laser intensities I_{532} at a different κ_{eff}.

We begin with the calculations of the nonlinear heating of the AuNS under the resonant CW plane wave illumination. The temperature T_{NP} of a spherical gold nanoparticle (with radius a) can be expressed as[7]

$$T_{\text{NP}} = T_0 + \frac{\epsilon_0 \omega}{2} \frac{3a^2}{\kappa_{\text{eff}}} |E_{\text{inc}}|^2 \frac{\epsilon_d^2}{\epsilon_m''(T_{\text{NP}})}, \tag{1}$$

where E_{inc} is the incident electric field, ω is the frequency of incident light, ϵ_d is the relative permittivity of the host medium, and $\epsilon_m''(T_{\text{NP}})$ is the imaginary part of the metal permittivity, which is described using the temperature-dependent Drude–Lorentz model[19]. The substantial increase of the temperature causes the imaginary part of the metal permittivity ϵ_m'' to change substantially, leading to the optical heating and the scattering responses becoming nonlinear at high light intensity. Moreover, the results in Fig. 2(b) show that the temperature evolution depends strongly on the thermal conductivity of the surrounding environment. This confirms that heat dissipation needs to be considered as it simultaneously competes with the temperature rise of the nanoparticle. Therefore, at the same laser intensity, the AuNS located in different thermal environments rises to different temperatures in a steady state.

Once the AuNS temperature is determined with respect to the laser intensity, one can calculate the scattering cross-section C_{sca} of the nanoparticle at certain incident irradiations. Figure 2(c) shows that the C_{sca} at the wavelength of 532 nm reduces remarkably through photothermal effect, and the modulation of C_{sca} is confirmed to be repeatable and reversible by observing the full recovery of the scattering intensities when the laser intensity switched back to the initial value[11]. As shown in Fig. 2(d), the reduction of C_{sca} results in the slowdown of the increase of scattering intensity. At low excitation intensities, the normalized scattering intensity from the 70-nm AuNS increases monotonically with the incoming intensity, with the slope that depends on the effective thermal conductivity of the environment in which the nanoparticles are located. At higher intensities, the scattering reaches saturation. The agreement between our theoretical and experimental results of the nonlinear saturated scattering confirms the photothermal nature of the scattering saturation. These results further imply that we have made a reasonable estimation of the effective thermal conductivities κ_{eff} for the several current media hosts. The heat dissipation is clearly effective for the silica-coated gold particles compared to the simple citrate stabilized ones in the oil immersion. The thicker silica shell provides more effective heat dissipation and the corresponding thermal properties become closer to that in SOG encapsulation.

Based on the nonlinear plasmonic scattering behavior, we performed the super-resolution imaging of the nanoparticles and the results are shown in Fig. 3. The schematic of the super-resolution optical imaging using suppression of scattering imaging (SUSI) microscopy[10,11] is shown in the inset box of Fig. 3(a). Briefly, the plasmonic scattering in the nanoparticles was excited by a Gaussian-shaped beam of 561 nm. In the meantime, the scattering signals at the periphery of the focal spot were suppressed by an intense donut-shaped beam of 532 nm, and finally a sub-diffraction limit image spot was achieved.

Figure 3(a) shows the scattering images of the bare AuNSs and AuNSs coated with the 40-nm silica shell, demonstrating more and more squeezed FWHM of the image spots obtained at growing intensities of the donut beam. More importantly, benefiting from the effective heat dissipation of the silica shell, the core-shell nanoparticles exhibit better thermal stability under the strong laser irradiation. We experimentally observed that when the laser intensity was larger than 0.8 MW/cm^2, the bare AuNSs were no longer thermally stable with the occurrence of deformation or even fragmentation. The best lateral feature size in the SUSI image is thus limited to 72 nm. In contrast, the shell-coated gold particles can withstand higher optical power and a deep subwavelength point spread function (PSF) approaching 50 nm can be successfully obtained, which is far smaller than the physical size of the particle itself. This indicates that the scattering does not report the shape of the nanostructure but rather the spatial origin of the scattering.

It is worth noting that, during the sample preparation, most of the particles are isolated and well separated. At the same time, pairs of nanoparticles can also be formed randomly. As shown in Fig. 4, we used correlated super-resolution SUSI and SEM to

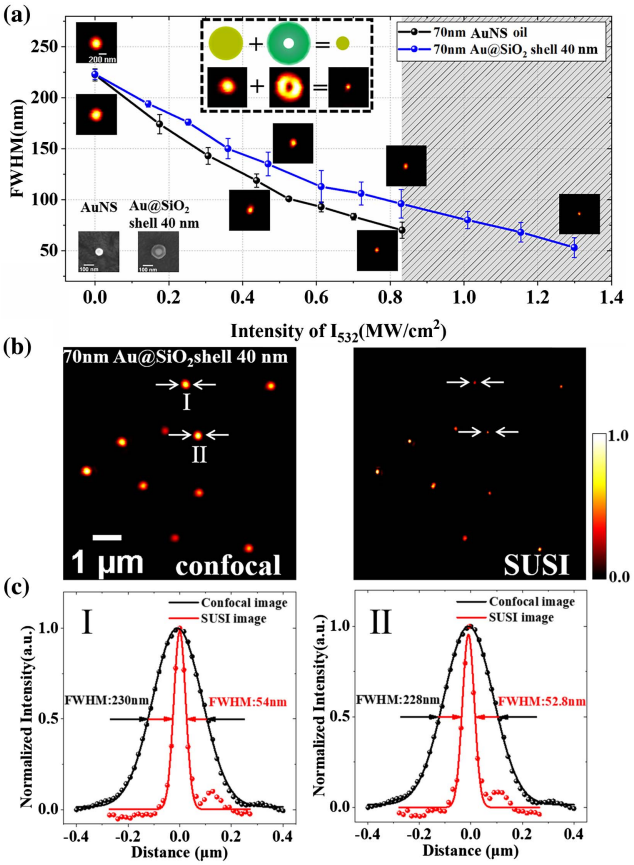

Fig. 3. (a) The FWHM of the scattering image spots using bare AuNSs and 40-nm-shell-coated AuNSs, with increasing suppression beam intensity I_{532}. A series of images with various suppression beam powers were taken, allowing for the quantification of the resolution dependence on the applied suppression power. The mean spot sizes for each power setting were determined by measuring the FWHM of the Gaussian-fitted profiles of individual nanoparticles and averaging over ten particles. The SEM of bare gold and Au@SiO_2 dispersed on the ITO substrate was performed for characterization. The SEM images were also shown in the figure. The region enclosed by the shaded area only involves the SUSI of 40-nm-shell-coated AuNSs. For the intensity larger than 0.8 MW/cm^2, the bare AuNSs were no longer thermally stable. (b) Confocal and SUSI microscopy imaging of isolated 40-nm-shell-coated AuNSs. (c) The intensity lateral profile of the selected nanoparticles (numbered by I and II). Discrete circle points are measured intensity profiles, and the solid lines are Gaussian fits.

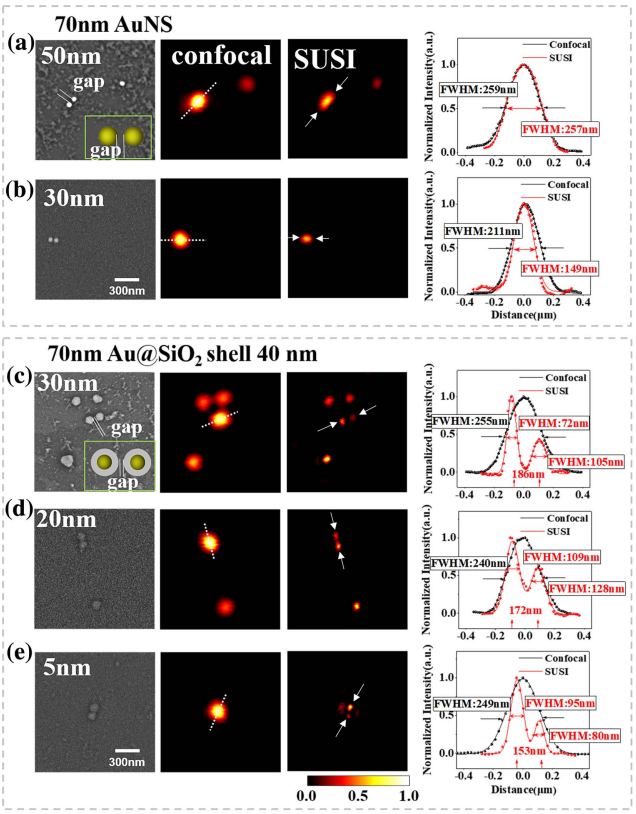

Fig. 4. Correlated super-resolution SUSI and SEM images for (a), (b) two closely spaced bare AuNSs and (c)–(e) pairs of 40-nm-shell-coated AuNSs. The gap-to-gap distances of two nanoparticles are shown in the SEM images. The super-resolution imaging of the shell-isolated nanoparticles clearly shows the resolving ability to distinguish two nanoparticles that are closely located in sub-diffraction spaces as small as 5 nm. The rightmost column plots the cross section profiles of the scattering images in confocal and SUSI.

study the resolving capability of the pairs of nanoparticles of various interparticle distances, demonstrating the effective spacing produced by the silica shells for reliable super-resolution imaging. The identification of the same particles in the SEM images and the optical scanning images was achieved via the pattern-matching method. In brief, we first used a femtosecond laser to write the markers on the glass slide, then deposited the nanoparticles, and then used SEM to observe and select the pairs of nanoparticles with specific spacings. Finally, we turned to the microscope system to record the super-resolution imaging of these particles. Due to the non-conductivity nature of the glass substrate, the SEM images in Fig. 4 have no good contrast for the silica shells of the core-shell particles. Nonetheless, we have already characterized these nanoparticles using transmission electron microscopy (TEM) along with SEM. In Fig. 3(a), we clearly see the gold core and silica shell in the SEM image as the nanoparticles are on the ITO substrate, which has good conductivity.

The correlating measurements combining SUSI and SEM can help to unravel, on a microscopic level, the influence of the silica shell on the resolution of super-resolution imaging. In Figs. 4(a) and 4(b), for the bare AuNSs, the two particles having gap-to-gap distances smaller than 50 nm, are no longer distinguishable. Specifically, in the confocal imaging with low light power, the images are diffraction-limit Gaussian-shaped spots, while in SUSI, they become elliptical along the arrangement direction of the two particles but are still indistinguishable. This suggests that when two nanoparticles are too close, individual nanoparticles may not be resolved due to plasmon coupling, i.e., the spatial origin of the scattering might shift to the gap center between the two particles (localized hot spot). On the contrary, pairs of core-shell particles can be readily resolved with the

gap-to-gap distance of 30 nm, 20 nm, and even down to 5 nm (almost linked). This is because the 40-nm-thick silica shell provides sufficient gap spacings of the two gold cores. The nanoscale gaps can be retrieved via line profile analysis in the SUSI images and present perfect consistency with the gap distances visible in the SEM images [Figs. 4(c)–4(e)].

We remark here that, the photothermal imaging speed is determined by the time scale of heating up and cooling down the nanoparticles. According to the previous study of nonlinear scattering using pulsed-beam irradiation[15], the response time of the approximate heating/cooling is on a 20-ns time scale. In our experiments, the imaging speed is about 1 second per frame, associated with a pixel dwell time of 10 μs. Therefore, the optical switching and the imaging are measured with the nanoparticles reaching the thermal equilibrium. A reduced laser-pulse width was obtained in previous attempts, showing a tradeoff effect between high-speed operation and modulation depth[10]. As a final remark, with the advances in materials science, silica coatings are mature to prepare, offering high biocompatibility and low toxicity for bioimaging and biomedical usage[20]. Additionally, high colloidal stability is another key importance. Aggregation and eventual fusion of metal nanoparticles are well known to induce drastic changes in the plasmonic properties and a significant loss of activity, in particular at high temperatures. Plasmonic metal nanoparticles with silica coating have proved to be good solutions to this problem[21,22]. Hence, we experimentally show that core–shell particles improve super-imaging properties by efficiently preventing the plasmon coupling caused by particle aggregation.

4. Conclusion

In conclusion, we investigated the nonlinear scattering of 70-nm-diameter gold nanospheres in different local surrounding media (i.e., immersed in oil, coated with silica shells, and encapsulated in SOG materials), as a function of laser intensity subjected to CW-laser illumination. We found that the particles' temperature elevation and scattering intensities with increasing laser intensity had a strong dependence on local heat dissipation associated with the effective heat conductivity of the complex environment. Gold nanospheres coated with silica shells show better heat resistance and thermal stability, which we use as robust plasmonic nanoprobes for super-resolution optical imaging using SUSI microscopy. Super-resolution imaging of gold nanospheres coated with a 40-nm-silica shell has been achieved with a lateral feature size of 52 nm ($\lambda/10$). Correlated SUSI and SEM measurements have revealed that the efficient gap spacing provided by the silica shell enables the resolution of core-shell particles with sub-diffraction distance down to gap-to-gap distance of 5 nm. Our work sheds light on the crucial role that the local thermal environment involving heat dissipation plays in nonlinear plasmonic scattering, and further extends the practical applications of the far-field super-resolution optical imaging of the shell-coated metal nanoparticles based on nonlinear plasmonic scattering.

Acknowledgement

This work was supported by the National Natural Science Foundation of China (No. 61805107) and National Key R&D Program of China (No. 2021YFB2802003).

References

1. P. K. Jain, K. S. Lee, I. H. El-Sayed, and M. A. El-Sayed, "Calculated absorption and scattering properties of gold nanoparticles of different size, shape, and composition: applications in biological imaging and biomedicine," J. Phys. Chem. B **110**, 7238 (2006).
2. L. Wang, M. Hasanzadeh Kafshgari, and M. Meunier, "Optical properties and applications of plasmonic-metal nanoparticles," Adv. Funct. Mater. **30**, 2005400 (2020).
3. K. A. Willets, A. J. Wilson, V. Sundaresan, and P. B. Joshi, "Super-resolution imaging and plasmonics," Chem. Rev. **117**, 7538 (2017).
4. Y.-L. Tang, T.-H. Yen, K. Nishida, J. Takahara, T. Zhang, X. Li, K. Fujita, and S.-W. Chu, "Mie-enhanced photothermal/thermo-optical nonlinearity and applications on all-optical switch and super-resolution imaging [Invited]," Opt. Mater. Express **11**, 3608 (2021).
5. S.-W. Chu, T.-Y. Su, R. Oketani, Y.-T. Huang, H.-Y. Wu, Y. Yonemaru, M. Yamanaka, H. Lee, G.-Y. Zhuo, M.-Y. Lee, S. Kawata, and K. Fujita, "Measurement of a saturated emission of optical radiation from gold nanoparticles: application to an ultrahigh resolution microscope," Phys. Rev. Lett. **112**, 017402 (2014).
6. S.-W. Chu, H.-Y. Wu, Y.-T. Huang, T.-Y. Su, H. Lee, Y. Yonemaru, M. Yamanaka, R. Oketani, S. Kawata, S. Shoji, and K. Fujita, "Saturation and reverse saturation of scattering in a single plasmonic nanoparticle," ACS Photonics **1**, 32 (2014).
7. Y. Sivan and S.-W. Chu, "Nonlinear plasmonics at high temperatures," Nanophotonics **6**, 317 (2017).
8. I. W. Un and Y. Sivan, "Thermo-optic nonlinearity of single metal nanoparticles under intense continuous wave illumination," Phys. Rev. Mater. **4**, 105201 (2020).
9. K. Nishida, G. Deka, N. I. Smith, S.-W. Chu, and K. Fujita, "Nonlinear scattering of near-infrared light for imaging plasmonic nanoparticles in deep tissue," ACS Photonics **7**, 2139 (2020).
10. H.-Y. Wu, Y.-T. Huang, P.-T. Shen, H. Lee, R. Oketani, Y. Yonemaru, M. Yamanaka, S. Shoji, K.-H. Lin, C.-W. Chang, S. Kawata, K. Fujita, and S.-W. Chu, "Ultrasmall all-optical plasmonic switch and its application to superresolution imaging," Sci. Rep. **6**, 24293 (2016).
11. J. Xu, T. Zhang, S. Yang, Z. Feng, H. Li, D. Hu, F. Qin, X. Ouyang, Y. Cao, L. Jiang, and X. Li, "Plasmonic nanoprobes for multiplexed fluorescence-free super-resolution imaging," Adv. Opt. Mater. **6**, 1800432 (2018).
12. X. Ouyang, F. Qin, Z. Ji, T. Zhang, J. Xu, Z. Feng, S. Yang, Y. Cao, K. Shi, L. Jiang, and X. Li, "Invited Article: saturation scattering competition for non-fluorescence single-wavelength super-resolution imaging," APL Photonics **3**, 110801 (2018).
13. C. Li, Y. Li, Y. Han, Z. Zhang, Y. Li, W. Wang, X. Hao, C. Kuang, and X. Liu, "Pulsed saturated absorption competition microscopy on nonbleaching nanoparticles," ACS Photonics **7**, 1788 (2020).
14. Y.-T. Chen, P.-H. Lee, P.-T. Shen, J. Launer, R. Oketani, K.-Y. Li, Y.-T. Huang, K. Masui, S. Shoji, K. Fujita, and S.-W. Chu, "Study of nonlinear plasmonic scattering in metallic nanoparticles," ACS Photonics **3**, 1432 (2016).
15. X. Zhang, J. Wang, S. Lamon, M. Gu, and Q. Zhang, "Scattering suppression in plasmonic nanostars using pulsed-beam irradiation for super-resolution optical imaging," Opt. Lett. **47**, 4223 (2022).
16. J. Kameoka, S. S. Verbridge, H. Liu, D. A. Czaplewski, and H. G. Craighead, "Fabrication of suspended silica glass nanofibers from polymeric materials using a scanned electrospinning source," Nano Lett. **4**, 2105 (2004).
17. K. Setoura, Y. Okada, D. Werner, and S. Hashimoto, "Observation of nanoscale cooling effects by substrates and the surrounding media for single gold nanoparticles under CW-laser illumination," ACS Nano **7**, 7874 (2013).
18. G. P. Zograf, M. I. Petrov, D. A. Zuev, P. A. Dmitriev, V. A. Milichko, S. V. Makarov, and P. A. Belov, "Resonant nonplasmonic nanoparticles

for efficient temperature-feedback optical heating," Nano Lett. **17**, 2945 (2017).
19. A. Alabastri, S. Tuccio, A. Giugni, A. Toma, C. Liberale, G. Das, F. De Angelis, E. Di Fabrizio, and R. P. Zaccaria, "Molding of plasmonic resonances in metallic nanostructures: dependence of the non-linear electric permittivity on system size and temperature," Materials **6**, 4879 (2013).
20. C. Hanske, M. N. Sanz-Ortiz, and L. M. Liz-Marzán, "Silica-coated plasmonic metal nanoparticles in action," Adv. Mater. **30**, 1707003 (2018).
21. N. T. Urban, M. R. Foreman, S. W. Hell, and Y. Sivan, "Nanoparticle-assisted STED nanoscopy with gold nanospheres," ACS Photonics **5**, 2574 (2018).
22. E. Cortés, P. A. Huidobro, H. G. Sinclair, S. Guldbrand, W. J. Peveler, T. Davies, S. Parrinello, F. Görlitz, C. Dunsby, M. A. K. Neil, Y. Sivan, I. P. Parkin, P. M. W. French, and S. A. Maier, "Plasmonic nanoprobes for stimulated emission depletion nanoscopy," ACS Nano **10**, 10454 (2016).